Synthesis of epitaxial ternary $Co_{1-x}Fe_xSi_2$ silicides with CsCl- and CaF_2-type cubic structures on Si(111) by codeposition techniques

S. Hong, C. Pirri, P. Wetzel, and G. Gewinner

Laboratoire de Physique et de Spectroscopie Electronique, Faculté des Sciences et Techniques 4, rue des Frères Lumière,
68093 Mulhouse Cédex, France

We have grown ternary $Co_{1-x}Fe_xSi_2$ silicide films, about 100 Å thick, by codeposition onto Si(111) held at room temperature in the whole composition range $0 \leq x \leq 1$. Low-energy electron diffraction, inelastic medium-energy electron diffraction, x-ray diffraction, x-ray photoelectron diffraction, and photoemission spectroscopy techniques are used to investigate the atomic and electronic structure of these ternary silicides. It is found that the as-deposited films are metallic and adopt an ordered cubic structure of CsCl type with essentially random vacancies, except in Co-rich films ($x \leq 0.25$) where a tendency toward an ordered vacancy arrangement of the CaF_2 type is already visible. Upon annealing at 650 °C, these silicides are found to be metastable, but phase separation does not take place. Fe-rich ($x \geq 0.85$) films invariably convert into a semiconducting phase with a structure similar to the orthorhombic β-$FeSi_2$ one. Yet, most interestingly, the cubic structure is preserved for $x \leq 0.85$, i.e., stabilized when the Co content exceeds about 15%. X-ray diffraction reveals that these phases exhibit partial CaF_2 long-range order. The order parameter is close to zero for $x = 0.85$ and increases rapidly with increasing Co content. The data indicate that Fe does not merely substitute for Co atoms in a perfect CaF_2-type $CoSi_2$ structure. Several of the Fe and possibly Co atoms preferentially occupy the interstitial octahedral sites of this latter structure even for $x \leq 0.50$, while for $x \geq 0.75$ a local environment essentially similar to that in defected CsCl-type structure is observed for both Fe and Co sites. [S0163-1829(97)01019-9]

I. INTRODUCTION

Epitaxial growth of crystalline materials has been a highly successful approach to preparing metastable systems, clarifying and understanding their various structural and electronic properties. Moreover, epitaxial growth of materials such as transition-metal silicides on silicon paves the way for high-speed silicon-integrated devices. Among silicides, Ni, Co, and Fe disilicides have been attracting attention more particularly for possible applications. The use of $CoSi_2$ silicide as a good conductor in metal-insulator (MI) devices is actually prominent. Indeed, using CaF_2 insulator barriers and $CoSi_2$ metal wells on Si(111), the first MI hot-electron transistor,[1] resonant-tunneling diode,[2] resonant-tunneling transistor,[3] and resonant-tunneling hot-electron transistor have been recently reported.[4]

Stable $CoSi_2$ disilicide has a fluorite (CaF_2) structure with a lattice constant of 5.365 Å, which is 1.2% smaller than that of silicon. Epitaxy of this binary silicide has been extensively studied. Due to their simple structure and small misfit relative to Si substrates, $CoSi_2$ films can be epitaxially grown on Si(111) with a high crystalline quality.[5] As to iron silicides, the Fe-Si system has a more complex bulk phase diagram, and $FeSi_2$ crystallizes in two different structures. The semiconducting $FeSi_2$ does not crystallize in the CaF_2 type, but in an orthorhombic structure with lattice parameters $a = 7.791$ Å, $b = 7.883$ Å, and $c = 9.863$ Å (stable below ~ 950 °C).[6] This complex form, labeled β-$FeSi_2$, displays 48 atoms in a unit cell, and may be obtained by a Jahn-Teller distortion of CaF_2-type structure. Actually, the morphology of β-$FeSi_2$ layers epitaxially grown on Si(111), despite much

work done, remains mediocre due to a poor matching of the orthorhombic cell to the hexagonal symmetry of the Si(111) surface as well as rotationally equivalent domain formation. On the other hand, there exists a metallic form of $FeSi_2$ labeled α-$FeSi_2$ stable at high temperatures (above ~ 950 °C) in a tetragonal structure with lattice parameters $a \approx 2.69$ Å and $c \approx 5.09$ Å.

Besides stable phases, it was recently reported that metastable $FeSi_{1+x}$ and $CoSi_{1+x}$ silicides can be epitaxially stabilized on Si(111) over the whole composition range $0 \leq x \leq 1$.[7–9] These metastable silicides adopt the so-called defect CsCl-type FeSi and CoSi structures, where only a fraction of metal sites is randomly occupied for $x > 0$. The metastable $FeSi_2$ an $CoSi_2$ phases with defected CsCl-type structure are stable up to ~ 400 °C. In the case of ultrathin films (< 30 Å), an α-$FeSi_2$-derived structure[10–13] has been obtained at about 500 °C. On the other hand, Onda *et al.* have reported the formation of a CaF_2-type γ-$FeSi_2$ phase grown on Si(111) under very particular growth conditions.[14]

A semiconducting β-$FeSi_2$ phase may be a promising candidate for optoelectronic applications in silicon-intergrated devices. Indeed, optical as well as electrical measurements[15,16] showed a direct gap of about 0.85 eV. However, the nature of the gap, direct or indirect, has not yet been established without doubt since one suspects, both theoretically and experimentally, the existence of an indirect gap, slightly lower than the direct one.[17,18] Very recently, using semiempirical tight-binding calculations in a continuous distortion of the γ-$FeSi_2$ into β-$FeSi_2$ phase, Miglio and Malegori[19] showed a strong structure sensitivity of the nature of the gap. Indeed, allowing for a slight decrease in the first-

<u>55</u>   13 040

neighbor distance, the nature of the gap becomes direct. Hence the doping effects induced by substitution of part of the Fe by Co atoms might well deeply alter the properties of the β-FeSi$_2$ layer. In this respect, Teichert *et al.*[20] reported the influence of Co doping on the physical properties of $Fe_{1-x}Co_xSi_2$ ($0 < \times \leq 0.05$) grown on insulating quartz substrates. The results indeed show a direct gap with linear band-gap reduction versus Co doping along with a change of conduction type from n to p. To our knowledge, the possibility to grow epitaxially ternary $Fe_{1-x}Co_xSi_2$ silicides on silicon and their relevant atomic and electronic structures have not yet been investigated in a systematic way. Motta and Christensen[21] performed a self-consistent total-energy calculation of ternary $Co_{1-x}Fe_xSi_2$ alloys in CaF$_2$ form. It was found that these ternary systems exhibit total-energy minima at values of the equilibrium lattice parameter $a(x)$ that increase with increasing x. However, the difference in lattice parameters of extreme CoSi$_2$ and FeSi$_2$ compositions remains quite small ($\Delta a \approx 0.05$ Å). Experimentally, Tan *et al.*[22] recently reported the sequential-ion-implantation synthesis of a ternary silicide on Si(100) held at 350 °C with doses of 2×10^{17} Co/cm^2 and 1.5×10^{17} Fe/cm^2. An extended x-ray-absorption fine-structure study performed on such silicides suggested the formation of a single-phase silicide in which Fe substitutes for part of the Co in a CaF$_2$-type structure. Lately, a transmission electron microscopy (TEM) investigation of $Fe_{0.5}Co_{0.5}Si_2$ prepared by sequential equal-dose implantations of Co and Fe on Si(111) held at 350 °C has been reported.[23] It was also concluded that the as-implanted ternary $Fe_{0.5}Co_{0.5}Si_2$ alloy crystallizes in a CaF$_2$-type structure. Furthermore, phase separation into CaF$_2$-type $Fe_{1-x}Co_xSi_2$ and α-$Fe_xCo_{1-x}Si_2$ (with x close to 1) has been observed upon annealing up to 1000 °C, for such an Fe-to-Co ratio. However, neither the possibility of epitaxy nor the evolution of atomic and electronic structures over a large composition range ($0 \leq x \leq 1$) have yet been explored. In this respect, codeposition may be much more suitable than implantation techniques since it permits a careful control of the stoichiometry.

In this work, we report on cubic $Co_{1-x}Fe_xSi_2$ compounds epitaxially grown on Si(111) over the whole composition range $0 \leq x \leq 1$ using the room-temperature codeposition technique. The investigation of these ternary silicides has been carried out by means of low-energy electron diffraction (LEED), inelastic medium-energy electron diffraction (IMEED), x-ray-diffraction (XRD), x-ray photoelectron diffraction (XPD), and photoemission spectroscopy techniques. We demonstrate the formation of epitaxial ternary $Co_{1-x}Fe_xSi_2$ silicides, with good atomic order at all stoichiometries ($0 \leq x \leq 1$), when codeposited on Si(111) at room temperature. These silicides are all metallic, and adopt a cubic structure derived from the CsCl-type FeSi and CoSi structure in which only half of the metal sites are occupied at random. However, in Co-rich films ($x \leq 0.25$), a tendency toward an ordered vacancy arrangement of the CaF$_2$-type structure is already observed, even at room temperature. Thermal-evolution studies indicate that the atomic and electronic structures are preserved up to ~ 400 °C. Upon further annealing at about 600 °C–650 °C, the atomic and electronic structures are strongly affected depending on the Fe-to-Co ratio. Nevertheless, experimental data suggest that the sili-

cide composition is preserved without phase separation. These silicide layers exhibit a metallic character as well as cubic structure up to Fe contents as high as $x \approx 0.85$, with partial CaF$_2$-type long-range order as clearly attested by XRD measurements. For $x \gtrsim 0.90$, the films are transformed into Co-doped β-FeSi$_2$, i.e., an orthorhombic semiconducting phase similar to pure β-FeSi$_2$.

II. EXPERIMENTAL PROCEDURE

Epitaxial ternary $Co_{1-x}Fe_xSi_2$ silicides were prepared on Si(111) in a UHV chamber, with a base pressure of $\sim 10^{-10}$ mbar. Prior to loading into the preparation chamber, the Si(111) wafers were cleaned in ultrasonic bath of ethanol for 30 min and dried in flowing N$_2$ gas. In order to remove surface oxides and other contaminants, the substrates were first heated at a temperature below 400 °C for a few hours, and then flashed to 950 °C, with the residual pressure kept below $\sim 5.10^{-10}$ Torr during the whole process. In this way, we obtained contaminant-free surfaces with sharp (7×7) LEED patterns. Fe, Co, and Si were evaporated in the 1–2-Å/min range using stable homemade evaporators with appropriate crucibles. Stoichiometric fluxes of different elements were carefully controlled by a two-quartz-microbalance system. CoSi$_2$ template layers were first grown by deposition of a 2-Å Co layer followed by codeposition of 9 Å CoSi$_2$ at room temperature (RT) subsequently annealed at 550 °C, which results in a well-defined $p(1 \times 1)$ LEED pattern and sharp electron confinement states observed at ~ 0.5 eV by ultraviolet photoemission spectroscopy.[24] The technique based on disilicide template layers has been shown in previous work on binary Fe or Co silicides to result in substantially improved quality of the films.[25,26] Then 100 Å $Co_{1-x}Fe_xSi_2$ ($0 \leq x \leq 1$) were codeposited at RT for a series of stoichiometries.

The *in situ* experimental setup has been described in detail elsewhere.[7,8] As to the structural characterization of the films, we note that Fe $2p_{3/2}$ and Co $2p_{3/2}$ XPD measurements were obtained at the highest $\pm 1°$ angular resolution of the hemispherical analyzer with a high-power (1600 W) Al $K\alpha$ ($h\nu = 1486.6$ eV) x-ray source. High-resolution Si $2p$ core-level photoemission spectra were recorded using a monochromatized Al $K\alpha$ x-ray source with an overall energetic resolution about 450 meV. Experimental XPD data are compared to single-scattering-cluster (SSC) simulations with spherical-wave corrections.[9,27] In these simulations, we used a spherical sector-shaped cluster defined by its radius $R = 12$ Å and a cone of half-angle $\Psi_0 = 60°$ centered on the emitter with its axis along the emission direction. An effective mean free path of 10 Å was used for both Fe $2p_{3/2}$ (779 eV) and Co $2p_{3/2}$ (706 eV) emissions. Partial-wave phase shifts were generated for $l = 0 - 20$, using a muffin-tin potential.[27] IMEED maps[28] were collected at 800-eV primary energy using a conventional LEED optics. *Ex situ* high-resolution x-ray-diffraction $\Theta - 2\Theta$ scans were performed by means of a Phillips diffractometer with monochromatized Cu $K\alpha$ radiation and a sample rotation stage.

III. RESULTS AND DISCUSSIONS

A. LEED and IMEED

First we note that all ternary 100-Å $Co_{1-x}Fe_xSi_2$ layers ($0 \leq x \leq 1$) codeposited on Si(111) with template at room

temperature show a $p(1 \times 1)$ LEED pattern, proving that all these silicides are epitaxial and fairly well ordered. From observed LEED spot widths, one can infer coherent domains about 5–10 lattice parameters in width. Furthermore, IMEED diagrams, recorded at normal incidence with primary electron energy $E_p = 800$ eV, exhibit well-defined anisotropic intensity distributions, as shown in Fig. 1(a). It may be helpful to recall that these angular intensity distributions reflect the crystallographic structure, in a similar way as the atom-specific XPD technique at the same kinetic energy.[28] More specifically, structural information is obtained in a very direct way in real space, since the intensity modulations essentially give a forward projected image of the first coordination shells around a given atomic species. It is worth noting that all metastable iron silicides, from Fe_3Si, to $FeSi_2$, as well as $CoSi_x$ silicides, grow with the B-type orientation on Si(111),[7–9,25] i.e., the crystal lattice of the films is rotated by 180° around the Si(111) surface normal. In the present case, the epitaxial relationship between the as-codeposited $Co_{1-x}Fe_xSi_2$ films and Si substrate may be readily checked by comparing the IMEED diagrams with that of cubic $FeSi_2$.

IMEED diagrams obtained from ternary silicides as a function of x are found to be very similar to each other, with a characteristic threefold-symmetric pattern. We compare on the top of Fig. 1 the IMEED diagrams obtained from ternary $Co_{0.5}Fe_{0.5}Si_2$ ($x = 0.5$) and binary $FeSi_2$ ($x = 1$). The most striking feature is that the distribution of the intensity observed on the fluorescent screen for $Co_{0.5}Fe_{0.5}Si_2$ is quite similar to the one obtained from epitaxial binary $FeSi_2$ film codeposited on Si(111) at room temperature which is known to exhibit a defected CsCl-type cubic structure with B-type orientation.[7] Indeed, major but inequivalent intensity maxima are seen every 60° along the inner ring of the screen. Patterns are symmetric with respect to the (-101) planes, and made of two differently shaped broad features near polar angles close to 35° and 30°, with respect to the surface normal [111] ($\Theta = 0°$), along the $[1-21]$ and $[-12-1]$ azimuthal directions, respectively. The close similarity between CsCl-type $FeSi_2$ and $Co_{1-x}Fe_xSi_2$ ($0 \leq x \leq 1$) IMEED data immediately reveals that $Co_{1-x}Fe_xSi_2$ films grow epitaxially with a B-type orientation, and that the specific CsCl-type cubic structure observed for $x = 1$ seems to be essentially preserved over the whole composition range $0 \leq x \leq 1$. This might be readily explained if one assumes that Co atoms essentially substitute for Fe atoms in the cubic $FeSi_2$ lattice, and notes that Fe and Co atoms have similar complex scattering amplitudes for electron at 800 eV, as shown below. In order to test the stability of these ternary silicides, room-temperature codeposited films have been annealed at two different temperatures, namely, 400 °C and 650 °C, for 1-h duration.

Upon annealing at 400 °C, the IMEED diagram is not substantially changed, whatever the Fe-to-Co ratio. The IMEED diagrams are still quite similar over the whole composition. Figure 1(c) illustrates such a diagram recorded from a $Co_{0.5}Fe_{0.5}Si_2$ layer. In contrast, the silicide surface exhibits now a well-ordered $p(2 \times 2)$ LEED pattern, except for binary $CoSi_2$ that preserves the $p(1 \times 1)$ periodicity (not shown). Figure 1(d) shows the $Co_{0.5}Fe_{0.5}Si_2$ $p(2 \times 2)$ LEED pattern. Such a $p(2 \times 2)$ pattern is commonly observed on

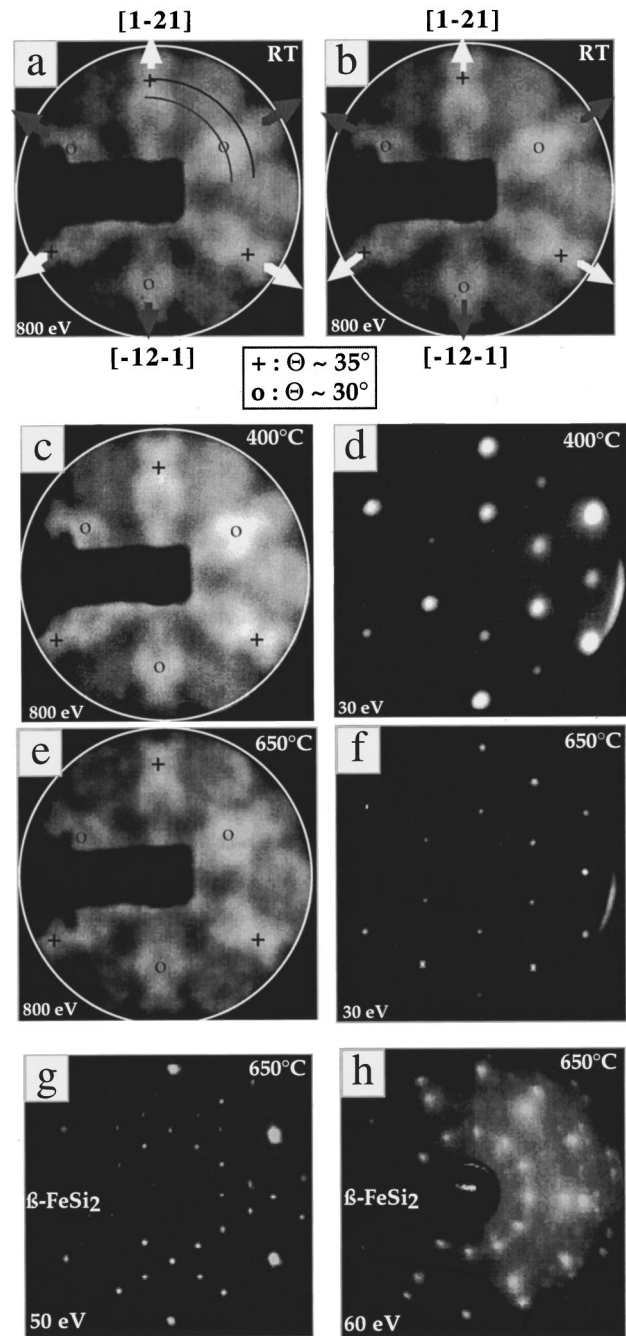FIG. 1. IMEED and LEED patterns at normal incidence of $FeSi_2$ and $Co_{0.5}Fe_{0.5}Si_2$. IMEED data have been recorded at primary energy $E_p = 800$ eV for codeposited (a) $FeSi_2$ and (b) $Co_{0.5}Fe_{0.5}Si_2$ on Si(111) at room temperature. (c) and (d) correspond to $Co_{0.5}Fe_{0.5}Si_2$ IMEED and LEED diagrams obtained upon annealing at 400 °C, respectively. (e) and (f) correspond to $Co_{0.5}Fe_{0.5}Si_2$ IMEED and LEED diagrams obtained upon annealing at 650 °C, respectively. Also shown are (g) (2×4) and (h) complex twelvefold-symmetry LEED patterns characteristic of multidomain β-$FeSi_2$ epitaxially grown on Si(111).

both CsCl-type $FeSi_2$ layers annealed at about 400 °C and thin (<30 Å) $FeSi_2$ films annealed at higher temperature, typically 500 °C–600 °C. In this latter case, the 2×2 superstructure was attributed to a Si segregation on top of the silicide film.[29]

Upon annealing at 650 °C, marked modification of both LEED and IMEED diagrams is observed, depending on the Fe-to-Co ratio. For $x \lesssim 0.85$, the threefold-symmetric IMEED diagram similar to that of Fig. 1(c) is preserved, thereby indicating that basically an epitaxial cubic structure closely related to the CsCl- and/or CaF$_2$-type persists as soon as Co content exceeds about 15%. Figure 1(e) displays the relevant Co$_{0.5}$Fe$_{0.5}$Si$_2$ IMEED diagram, which now exhibits an excellent contrast. However, at this stage on the sole basis of IMEED analysis, we cannot readily identify a structural transition, if any, similar to the one observed in the case of CoSi$_2$, which adopts its stable CaF$_2$-type structure upon annealing at about 500–650 °C.[7] Indeed, binary CaF$_2$-type CoSi$_2$ and ternary Co$_{1-x}$Fe$_x$Si$_2$ ($x \lesssim 0.85$) IMEED diagrams are very similar to each other. Actually, IMEED cannot readily distinguish between CsCl- and CaF$_2$-type structures since it mainly reflects nearest-neighbor bond directions. The $p(2 \times 2)$ LEED pattern persists and improves considerably. It now consists of very sharp diffraction spots, as shown in Fig. 1(f) for $x = 0.50$. This shows considerably improved short-range as well as long-range order upon annealing at 650 °C for $x \lesssim 0.85$. Note that the (2×2) superstructure spots, which are as sharp and narrow as the 1×1 spots obtained from the well-known CaF$_2$-type CoSi$_2$ ($x = 0$) surface, are clearly observed even for low Fe contents ($x = 0.10$). In sharp contrast, in the Fe-rich regime $x \gtrsim 0.90$, the LEED pattern converts into either a 2×4 [Fig. 1(g)] or a complex twelvefold-symmetry [Fig. 1(h)] diagram. Moreover, relevant IMEED modulations completely vanish, i.e., the diagram (not shown) consists of a diffuse homogeneous intensity background. Such diagrams are similar to that observed for multidomain β-FeSi$_2$ epitaxially grown on Si(111).[30] In the case of orthorhombic semiconducting β-FeSi$_2$ phase, the lack of IMEED anisotropy can be explained by the fact that, on one hand, the Jahn-Teller distortion of the CaF$_2$-type structure results in inequivalent sites that contribute to the intensity modulation with a series of different forward-scattering directions that completely destroy the IMEED modulations. On the other hand, three silicide orientations separated by a 120° rotation are equally likely to occur, on the grounds of the threefold symmetry of the substrate Si(111) surface and rectangular in-plane unit cell of the matching β-FeSi$_2$ planes. Moreover, different epitaxial relationships of β-FeSi$_2$ on Si(111) has been observed by means of TEM as well as transmission electron diffraction (TED) measurements.[31] It has been found that either the $(101)_{\beta\text{-FeSi2}}$ or $(110)_{\beta\text{-FeSi2}}$ plane may be parallel to the (111)Si plane with the azimuthal $[010]_{\beta\text{-FeSi2}}$ or $[001]_{\beta\text{-FeSi2}}$ direction aligned with $[-101]_{\text{Si}}$ or $[10-1]_{\text{Si}}$, respectively. Clearly, both LEED and IMEED data strongly suggest the formation of a structure of the β-FeSi$_2$ type, i.e., a metal-semiconductor phase transition for Fe-rich ($x \gtrsim 0.90$) ternary films annealed at about 650 °C. In order to confirm or disprove this point, ultraviolet photoelectron spectroscopy (UPS) measurements were carried out.

B. UPS measurements

In Fig. 2, we show a series of UPS spectra (He I) recorded at normal emission from codeposited 100-Å Co$_{1-x}$Fe$_x$Si$_2$ films as a function of x, after annealing at 400 and 650 °C.
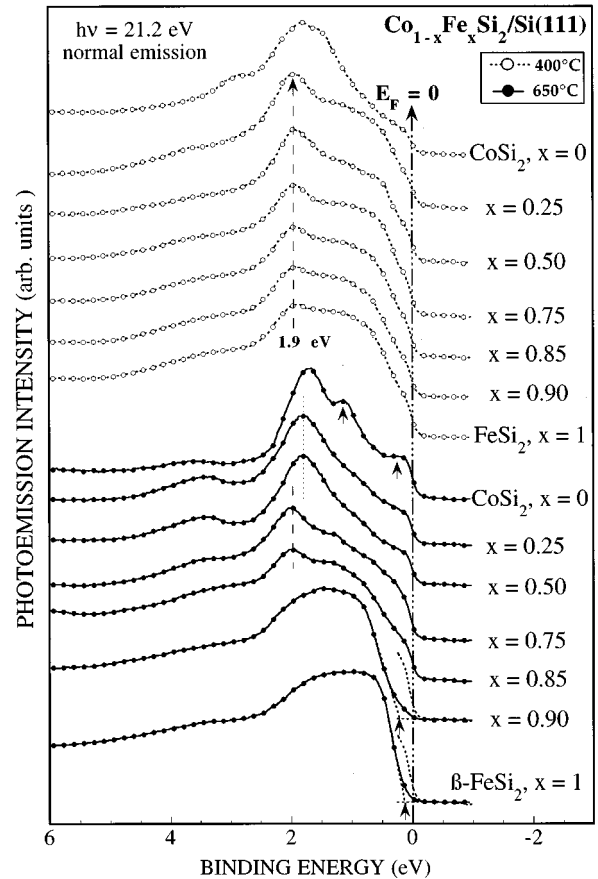

FIG. 2. UPS spectrum evolution of ternary 100-Å Co$_{1-x}$Fe$_x$Si$_2$ codeposited on Si(111) annealed at 400 °C and 650 °C as a function of x.

All spectra show a dominant feature at about $1-2$ eV binding energy which essentially reflects nonbonding iron and cobalt $3d$ bands and a broad shoulder in the $\sim 2-5$ eV binding-energy range that originates from bonding metal (Fe,Co)$3d$ and Si $3p$ states.[8,30] However, UPS is sensitive to both surface and bulk electronic properties of the film, and a detailed interpretation needs a more careful analysis. In particular, these ternary films exhibit surface states that will be considered elsewhere. The purpose of UPS spectra shown here is mainly to establish the metallic or semiconducting character of the films. This may be done by investigation of the density of state at the Fermi level. As can be seen, all UPS spectra obtained from ternary films annealed at 400 °C display a clearcut Fermi edge, indicating the formation of metallic ternary disilicides, irrespective of the Fe-to-Co ratio. However, upon annealing at 650 °C, the UPS spectra evolve differently as a function of x. A well-marked Fermi edge is still observed for Fe contents $x \lesssim 0.85$, while the opening of a band gap occurs for $x \gtrsim 0.90$ with a valence-band maximum located at about $0.1-0.2$ eV below the Fermi level E_F. The position of the valence-band maximum with respect to the Fermi level depends on the Co content. This means that 100-Å-thick ternary films with a Co content of 10% or less convert into a semiconducting phase. This is quite consistent with the change in structure observed by both LEED and IMEED. Finally, we note here that, when the Co content exceeds about 15%, ternary films are strongly stabilized in a
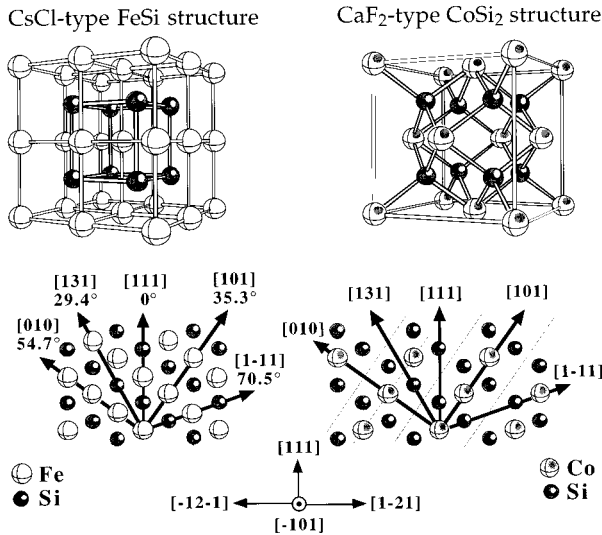
FIG. 3. Sketches of CsCl-type FeSi (left) and CaF$_2$-type CoSi$_2$ (right) structures with corresponding cross-sectional cuts through the (-101) plane. The arrows indicate expected directions and polar angles with respect to the [111] surface normal for forward-scattering enhancement of photoemission intensity.
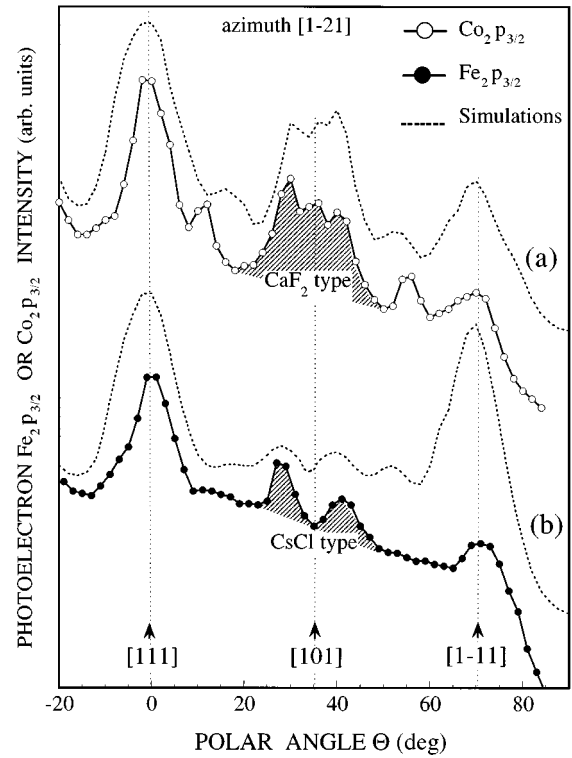

FIG. 4. Polar-angle scans of Co $2p_{3/2}$ (open circles) and Fe $2p_{3/2}$ (solid circles) photoelectron intensities from CaF$_2$-type CoSi$_2$ and CsCl-type FeSi$_2$ along the [$1-21$] azimuth with an angular resolution of $\pm 1°$ using classical Al K_0 source (1486.6 eV). Calculated single-scattering profiles (a) and (b) (dotted line) correspond to Co $2p_{3/2}$ (706 eV) and Fe $2p_{3/2}$ (779 eV) in CaF$_2$-type CoSi$_2$ and CsCl-type FeSi$_2$, respectively. The data are normalized to the same intensity at $\Theta = 0°$. The arrows indicate forward-scattering directions at nearest or next-nearest neighbors of the ordered CaF$_2$-type and CsCl-type FeSi structures shown in Fig. 3.

metallic epitaxial cubic structure, more adapted to the structure of the Si substrate than β-FeSi$_2$-type phases.

C. Reference x-ray photoelectron diffraction profiles

In order to obtain more information on the crystallographic structure of Fe$_{1-x}$Co$_x$Si$_2$ films, photoelectron-intensity (XPD) modulations of Fe $2p_{3/2}$ and Co $2p_{3/2}$ core levels have been measured as a function of polar angle using Al $K\alpha$ radiation. Since IMEED data show the same three-fold symmetry as the one of the defected CsCl-type FeSi$_2$ or CaF$_2$-type CoSi$_2$, these XPD polar profiles have been scanned through the (-101) plane along the two nonequivalent opposite azimuthal [$1-21$] and [$-12-1$] directions, along which major forward-focusing directions are expected. The CsCl-type FeSi and CaF$_2$-type CoSi$_2$ structures as well as their cuts through the (-101) plane are shown in Fig. 3. Note that in the zeroth-order interference (forward focusing) approximation, CsCl- and CaF$_2$-type XPD profiles give rise to the same forward-scattering peaks along [111], [101], [$1-11$], [131], and [010] atomic rows. Indeed, the defected CsCl-type FeSi$_2$ or CaF$_2$-type CoSi$_2$ can be derived from CsCl-type FeSi (CoSi) upon removing one out of two metal atoms. A defected CsCl-type structure consists of disordered metal vacancies as opposed to the CaF$_2$-type, where the vacancies are ordered in a specific way; i.e., within the $\langle -101 \rangle$ plane, every second [101] metal-atomic row is removed so that no nearest neighbor metal pairs are left, as sketched in Fig. 3. In this way, the lattice periodicity of defected CsCl-type FeSi$_2$ is similar to that of CsCl-type FeSi while for CaF$_2$-type CoSi$_2$ it becomes twice as large.

In order to go beyond the forward-focusing approximation and to distinguish between CsCl and CaF$_2$ atomic arrangements, it is useful first to consider the Fe $2p_{3/2}$ and Co $2p_{3/2}$ XPD profiles recorded from well-known binary FeSi$_2$ and CoSi$_2$ layers. Figures 4 and 5 display the reference-defected CsCl-type FeSi$_2$ (Fe $2p_{3/2}$) and

CaF$_2$-type CoSi$_2$ (Co $2p_{3/2}$) XPD profiles recorded along [$1-21$] and [$-12-1$] azimuthal directions, respectively. As mentioned above, both profiles exhibit forward-scattering structures centered at the same polar angles. Indeed, three prominent structures are observed near $\Theta = 0°$, $\Theta \approx 35°$, and $\Theta \approx 70°$ in the [$1-21$] direction, and around $\Theta = 0°$, $\Theta \approx 30°$, and $\Theta \approx 55°$ in the [$-12-1$] direction. All these particular polar angles coincide with forward-focusing directions shown in Fig. 3. However, these reference profiles can be clearly distinguished by the fine structure associated with higher-order interference effects occurring around [101] ($\sim 35°$) and [131] ($\sim 30°$) atomic rows along the [$1-21$] and [$-12-1$] azimuthal directions, respectively. Along the [101] atomic row, the CaF$_2$-type Co $2p_{3/2}$ profile exhibits a structure with strong anisotropy factor defined by $F = (I_{max} - I_{min})/I_{min}$ that shows three maxima located at $\Theta \approx 30°$, $\Theta \approx 35°$, and $\Theta \approx 40°$, whereas defected CsCl-type Fe $2p_{3/2}$ profile shows a volcano-shaped structure with a minimum instead of a maximum along [101] forward-scattering direction as well as a much smaller anisotropy factor. The physical reasons for the particular shape of the structure at $\Theta \approx 35°$ were extensively investigated in previous work.[8] Briefly, this effect is due to destructive interferences from out-of-chain atoms relatively close in angle to the [101] directions as well as to the reduction by a factor 2 of the
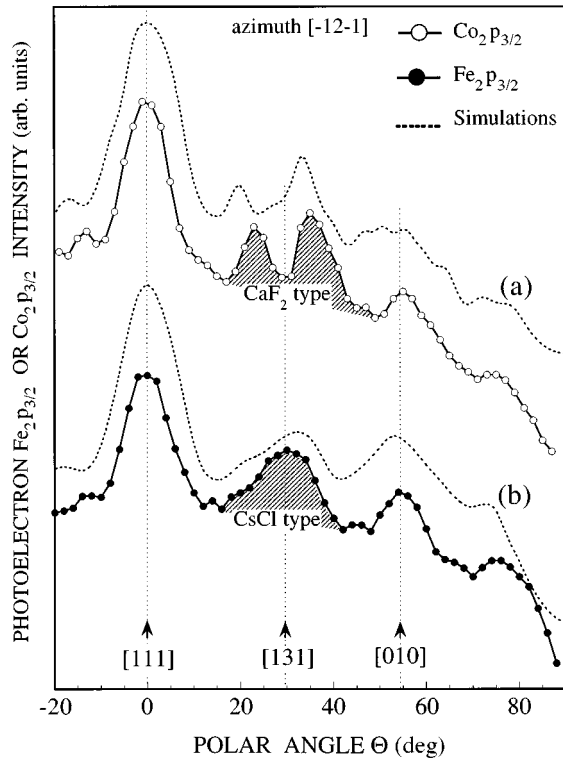
FIG. 5. Same as Fig. 4, but along the $[-12-1]$ azimuth.

FIG. 6. Calculated single-scattering Co $2p_{3/2}$ (706 eV) and Fe $2p_{3/2}$ (779 eV) profiles in the same crystallographic structure of defected CsCl type (FeSi$_2$ or CoSi$_2$).

atomic density along [101] rows in defected CsCl-type structure. It is worth noting that this particular splitting of the [101] forward-scattering feature is characteristic of the random-metallic-vacancy network in CsCl-type FeSi$_2$. Similarly, along the [131] atomic row, it is the CaF$_2$-type Co $2p_{3/2}$ profile that exhibits a volcano-shaped peak with a deep minimum in intensity along forward-scattering direction at $\Theta \approx 30°$, while a single asymmetric peak is formed in the case of defected CsCl-type FeSi$_2$. These specific features of the XPD are also fairly well reproduced by simulations we have performed using the cluster model in the single-scattering spherical-wave approximation for CsCl-type FeSi$_2$ and CaF$_2$-type CoSi$_2$ structures. Calculations at kinetic energies of 779 and 706 eV correspond to Fe $2p_{3/2}$ and Co $2p_{3/2}$ profiles, respectively. The calculated profiles (dotted lines) are compared to experiment in Figs. 4 and 5. As can be seen, simulation and experiment are in a good agreement in both polar-angle positions and overall shape and clearly exhibit the characteristic fine structure discussed above. This allows us to use these fingerprints to discriminate between CsCl- and CaF$_2$-type structures.

In order to make sure that the observed difference in fine structure along the [101] and [131] atomic rows between the two reference XPD profiles is actually due to a change in structure rather than the difference in chemical nature of the metal (Fe,Co) and photoelectron (Fe $2p_{3/2}$,Co $2p_{3/2}$) kinetic energy, we have performed single-scattering-cluster simulations in the same defected CsCl-type structure, namely, CsCl-type FeSi$_2$ and CoSi$_2$, for Fe $2p_{3/2}$ and Co $2p_{3/2}$ profiles as shown in Fig. 6. As can be seen, profiles related to Fe $2p_{3/2}$ and Co $2p_{3/2}$ are essentially the same. Therefore, these simulations clearly demonstrate that if Fe and Co atoms lie in the same local crystallographic environment, the
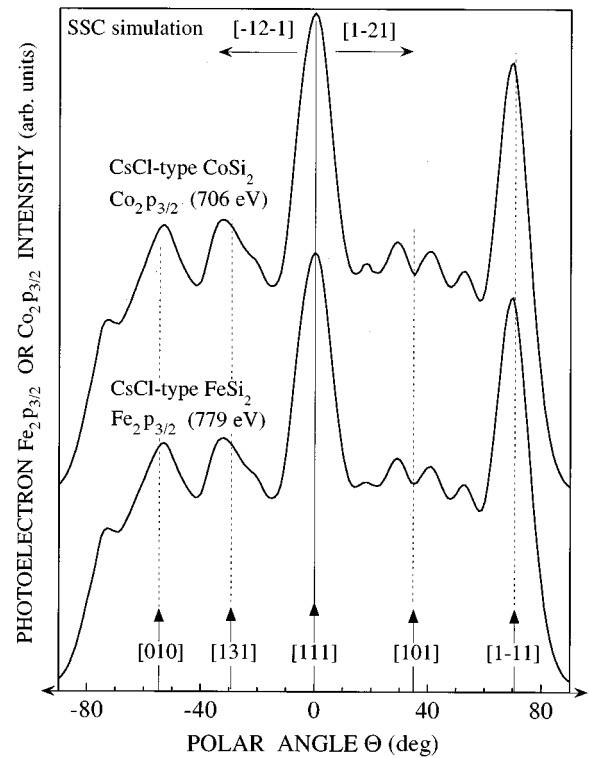
corresponding XPD profiles must be the same, irrespective of the Co or Fe nature of the occupied metal sites. This can be traced back to the fact that the calculated scattering factors (not shown) are very similar for Fe and Co, at the small scattering angles ($\leqslant 40°$) and high photoelectron kinetic energies (779 and 706 eV) involved. This indicates a metal-type independence (for neighbors in the first transition series) of the XPD profiles that reflect the CsCl and CaF$_2$-type geometric arrangement of the atomic species but not the chemical nature (Fe or Co) of the metal site. Hence we are now in a situation to take advantage of the reference CsCl and CaF$_2$-type profiles in the structural study of ternary Co$_{1-x}$Fe$_x$Si$_2$ phases.

D. X-ray photoelectron diffraction profiles for Co$_{1-x}$Fe$_x$Si$_2$

Fe $2p_{3/2}$ and Co $2p_{3/2}$ XPD profiles for codeposited Co$_{1-x}$Fe$_x$Si$_2$ silicides at room temperature along azimuthal $[1-21]$ and $[-12-1]$ directions are shown in Figs. 7 and 8, respectively. The most striking observation is that all profiles are essentially very similar to that of the reference CsCl-type profile. As discussed above, this close similarity leads immediately to the conclusion that all ternary silicides grown at room temperature have defected CsCl-type cubic structure in which Fe and Co atoms basically adopt the same local environment. Since phase separation is not likely to occur at room temperature because of reduced atomic mobility, it is expected that Fe and Co occupy the metal sites in defected CsCl-type structure in a random distribution with probabilities x and $1-x$, respectively. However, Co $2p_{3/2}$ profile related to Co-rich ($x \leqslant 0.25$) films shows a slight difference
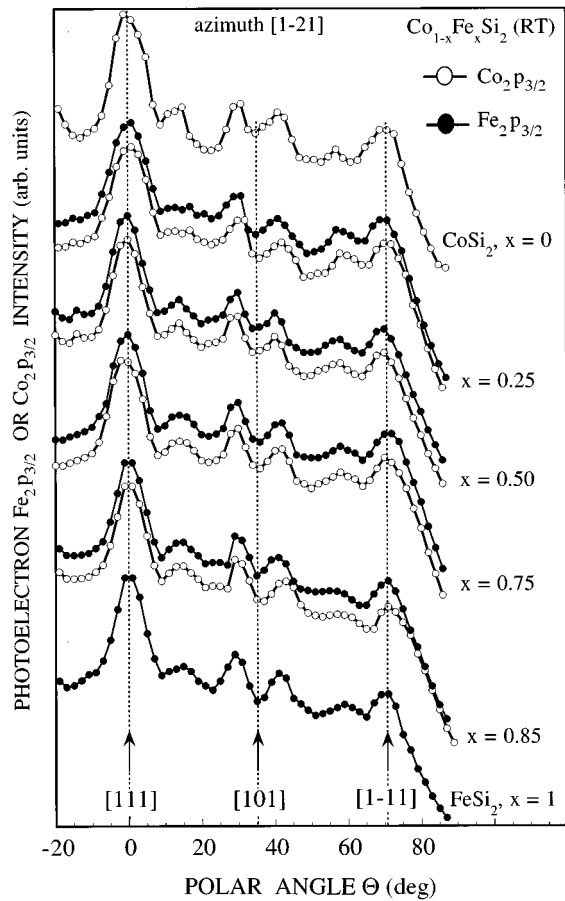
FIG. 7. Polar-angle scans of Co $2p_{3/2}$ (open circles) and Fe $2p_{3/2}$ (solid circles) photoelectron intensities from codeposited $Co_{1-x}Fe_xSi_2$ on Si(111) at room temperature as a function of x along the $[1-21]$ azimuth. The data are normalized to the same intensity at $\Theta = 0°$.

FIG. 8. Same as Fig. 7, but along the $[-12-1]$ azimuth.

concerning the fine structure around $\Theta = 30°$ (Fig. 8). Indeed, this structure exhibits a tendency to a double-peaked shape, intermediate between that in pure CsCl and CaF_2-type structures. This suggest that binary $CoSi_2$ as well as Co-rich ($x \leq 0.25$) ternary films codeposited at room temperature already exhibit a tendency toward a local ordered vacancy arrangement of the CaF_2 type. Nevertheless, high-resolution x-ray diffraction (HRXRD) Θ-2Θ scans (not shown) do not clearly show (111) reflections characteristic of the relevant CaF_2-type superstructure for room-temperature codeposited Co-rich ($x \leq 0.25$) films. The lack of such (111) reflections may be due to the mere absence of CaF_2-type long-range order and/or to a too small reflection intensity, on the grounds of low silicide thickness (100 Å) and small deviation from a statistical distribution of metal vacancies in defected CsCl-type structure. In this respect, it is interesting to recall the conclusions arrived at from extended x-ray-absorption fine-structure (EXAFS) measurements for room-temperature codeposited $CoSi_2$ and $FeSi_2$ films.[7,31] Metastable $CoSi_2$ EXAFS results are essentially similar to those of CsCl-type $FeSi_2$. The numerical data fitting procedure reveals that Co atoms are surrounded by 8($\pm$0.5) Si nearest neighbors at about 2.34 Å and by 3($\pm$1) Co nearest neighbors at about 2.68 Å as opposed to the CaF_2-type structure in which the nearest Co neighbors are located at about 3.8 Å.[7]
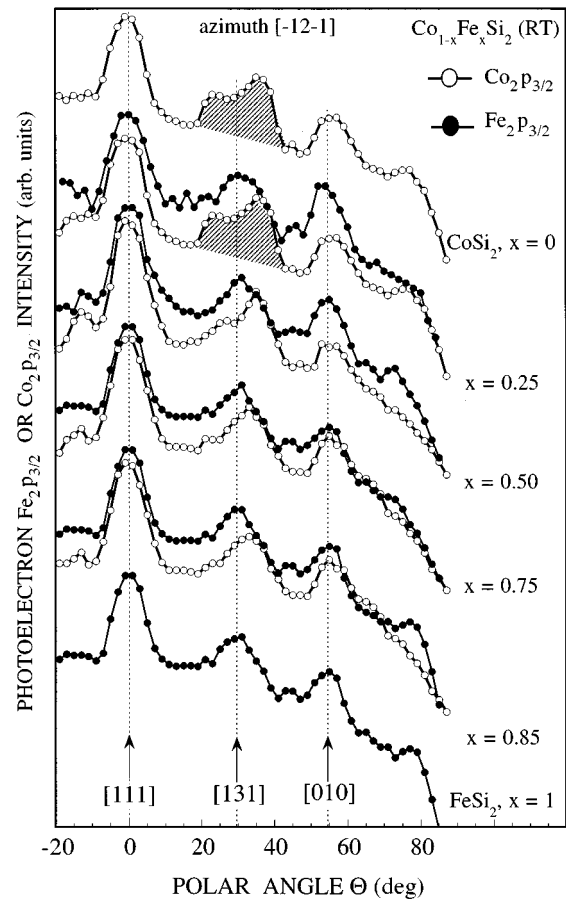
In ideal defected CsCl-type $CoSi_2$ with random vacancies, a statistical distribution gives rise to a mean value of three next-nearest neighbors at about 2.68 Å. In the case of a small deviation from a statistical distribution toward CaF_2-type order, as suggested by our XPD data, this average value must be lower than 3. However, no evidence could be obtained from EXAFS data of a deviation from statistical distribution which is thus probably small. It is well known that the EXAFS technique does not give precise coordination numbers since their extraction strongly depends on nonstructural parameters such as dynamic and static lattice disorder (Debye-Waller factor).

According to XPD data, this partial CaF_2 order does not evolve substantially upon annealing at about 400 °C. More generally, at this stage, the XPD profiles (not shown) do not exhibit any appreciable change, irrespective of Fe-to-Co ratio. This clearly indicates that the defected CsCl-type structure (with partial CaF_2-type order on the Co-rich side) is stable up to 400 °C for both binary ($x = 0$ and 1) and ternary disilicides. However, upon annealing at 650 °C, important changes take place in the XPD profiles, as shown in Figs. 9 and 10 for $[1-21]$ and $[-12-1]$ azimuths, respectively, indicating a change in atomic structure. For $x \geq 0.90$, XPD modulations (not shown) are no longer observed in agreement with IMEED results which confirm the transition toward the orthorhombic β-$FeSi_2$-type structure, as discussed in Sec. III A. The most striking observation, however, is that, for $x \leq 0.85$, well-defined XPD profiles are still observed, and reflect the persistence of an epitaxial cubic structure in
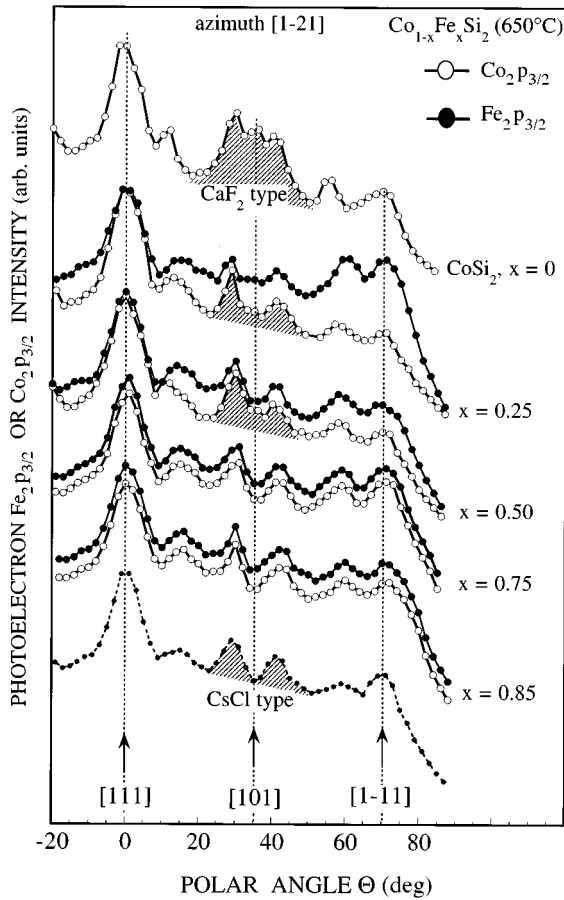
FIG. 9. Polar-angle scans of Co $2p_{3/2}$ (open circles) and Fe $2p_{3/2}$ (solid circles) photoelectron intensities from codeposited Co$_{1-x}$Fe$_x$Si$_2$ upon annealing at 650 °C as a function of $x \leqslant 0.85$ along the $[1-21]$ azimuth. The data are normalized to the same intensity at $\Theta = 0°$.

FIG. 10. Same as Fig. 9, but along the $[-12-1]$ azimuth.

the ternary films. *This again demonstrates that Co in excess of about 15% stabilizes the cubic structure of these silicides up to 650 °C.* More specifically for Fe content $x \geqslant 0.75$, the Co $2p_{3/2}$ and Fe $2p_{3/2}$ profiles remain similar to that of the reference defected CsCl-type reproduced at the bottom of Figs. 9 and 10. Hence we conclude that an Fe and Co local environment of defected CsCl type is essentially preserved up to 650 °C for $x \geqslant 0.75$. However, the Co $2p_{3/2}$ and Fe $2p_{3/2}$ profiles evolve differently when the Co content is about 50% or larger. Indeed, the Fe $2p_{3/2}$ profiles remain similar to the reference CsCl-type one for $x \approx 0.50$ and become intermediate between CsCl and CaF$_2$ types for $x \approx 0.25$ and below, whereas the Co $2p_{3/2}$ profiles clearly evolve toward that of the reference CaF$_2$-type. This clear-cut difference indicates that Fe and Co atoms now reside in different local environments for $x \leqslant 0.50$, i.e., Fe atoms adopt a CsCl-type local environment, while Co atoms prefer a CaF$_2$-type one. We also note that the Fe $2p_{3/2}$ profile related to Co$_{0.75}$Fe$_{0.25}$Si$_2$ silicide exhibits strong intensity enhancement at grazing emission angles, a behavior generally observed in the case of very thin films (~ 10 Å). This can be interpreted in terms of Fe segregation, and suggests a near-surface Fe enrichment, making the interpretation of the Fe $2p_{3/2}$ profile more complex for this Fe concentration. As to the Co $2p_{3/2}$ profiles for $x \leqslant 0.50$, we can see a marked
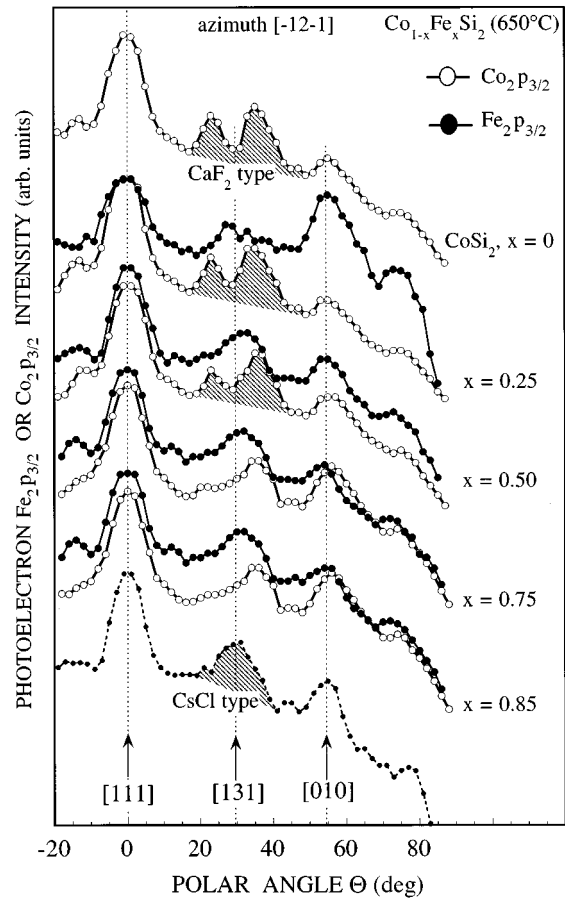
difference in fine structure around $\Theta = 35°$ with respect to that of the reference CaF$_2$-type profile. Indeed, the characteristic triple-peaked structure is partly transformed into a volcano-shaped one with a marked reduction in the anisotropy factor. The relative loss in forward-scattering intensity along the $[101]$ ($\Theta \approx 35°$) as compared to $[111]$ ($\Theta = 0°$) direction is particularly remarkable, as compared to the reference CaF$_2$-type profile. This feature may be qualitatively explained by the lack of some metal scatterers in the $[101]$ atomic row, thereby leading to a reduction in forward-scattering contributions along this row. Note that the metal-site occupation probabilities in the $[101]$ atomic row are 50% and 100% in the case of CsCl-type FeSi$_2$ and CaF$_2$-type CoSi$_2$, respectively. In contrast, along $[111]$, the nearest-neighbor scatterer is the Si atom present in both structures. Thus the attenuation of the XPD intensity at $\Theta = 35°$ suggests that annealing Co-rich Co$_{1-x}$Fe$_x$Si$_2$ films at about 650 °C does not lead to a perfect CaF$_2$-type structure, in contrast with pure CoSi$_2$ film. *Only partial CaF$_2$ order seems to be achieved even for low Fe content*, i.e., interstitial octahedral sites in a perfect CaF$_2$-type structure are occupied by a fraction of metal atoms, probably mainly Fe atoms since the Fe $2p_{3/2}$ profile more closely resembles the defected CsCl type. Moreover, we observe a systematic reduction up to 15% in overall XPD anisotropy with respect to CoSi$_2$ (not apparent in the normalized data presentation of Figs. 7–10). This suggests a marked increase in static disorder, i.e., a local distortion of the cubic structure brought about by the Fe atoms when introduced into the CoSi$_2$ structure. Finally, let
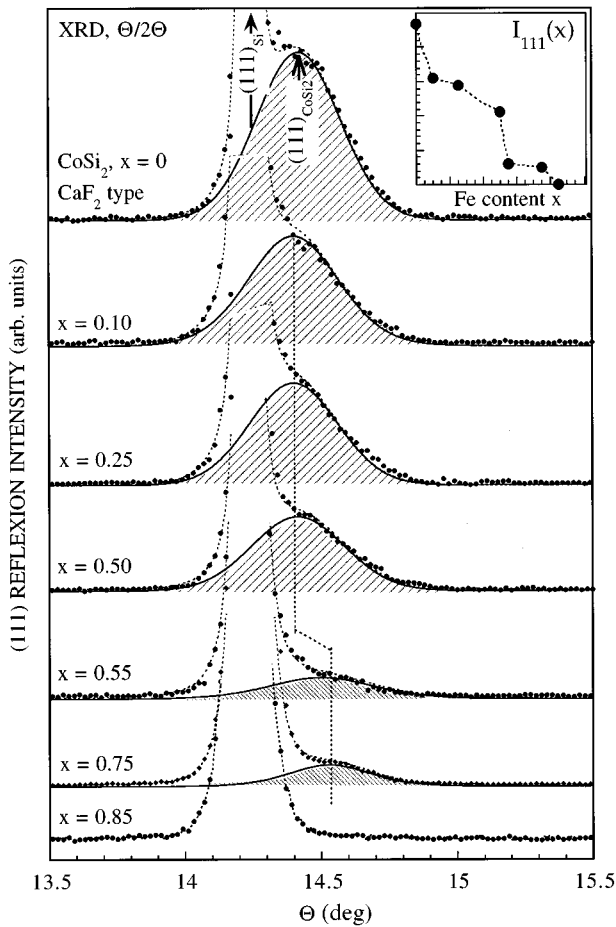
FIG. 11. HRXRD Θ-2Θ measurements for $Co_{1-x}Fe_xSi_2$ ($0 \leqslant x \leqslant 0.85$) annealed at 650 °C scanned from $\Theta = 13.5°$ to $\Theta = 15.5°$ corresponding to (111) reflections region of Si(111) substrate or CaF_2-type $CoSi_2$(111).

us emphasize that the present XPD data clearly demonstrate that an ideal CaF_2-type structure where the Fe merely substitutes for Co, as considered in previous theoretical calculations, is not formed. The above interpretation assumes that phase separation does not take place upon annealing at 650 °C. From the XPD data at hand, we can rule out phase separation into pure CaF_2-type $CoSi_2$ and defected CsCl-type $FeSi_2$, since the Co $2p_{3/2}$ XPD profile always shows substantial deviations from the reference CaF_2-type structure. In order to gain more insight into the degree of CaF_2-type long-range order as a function of Fe content, a detailed XRD study is desirable. As a first step in this study we have carried out XRD $\Theta - 2\Theta$ scans of the (111)-reflection characteristic of the relevant CaF_2-type superstructure for typical films with a cubic structure ($x \leqslant 0.85$) annealed at 650 °C.

E. X-ray-diffraction results

Figure 11 displays HRXRD $\Theta - 2\Theta$ measurements for $Co_{1-x}Fe_xSi_2$ ($0 \leqslant x \leqslant 0.85$) annealed at 650 °C scanned from $\Theta = 13.5°$ to $\Theta = 15.5°$, which corresponds to the (111)-reflection region of the Si(111) substrate or CaF_2-type $CoSi_2$(111). The (111)-reflection peak of silicon substrate at $\Theta \approx 14.23°$, labeled (111)$_{Si}$ is truncated. Note that upon referring all indexes to the simple cubic system with lattice

parameters equal to that of silicon substrate, the (111) reflection is forbidden in the CsCl-type structure. The main observation is that (111)$_{silicide}$ reflection occurs for $x \leqslant 0.75$, i.e., all ternary films exhibit CaF_2-type long-range order when the Co content exceeds 25%. However, the (111)-reflection intensity $I(x)$ decreases steadily with increasing Fe content x, and eventually vanishes near $x = 0.50$. This decrease, relative to the one of a CaF_2-type $CoSi_2$ (I_0), may be attributed to a change in crystallographic structure brought about by the Fe atoms, as shown by the XPD and/or to a change in static and dynamic disorder as a function of Fe content x. However, the dynamic disorder contribution does not depend substantially upon the Fe content x, since tight-binding calculations[32] show that elastic constants of $FeSi_2$ and $CoSi_2$ in CaF_2 form are quite similar. In contrast, concerning the static lattice disorder one expects indeed an enhanced contribution corresponding to distortions brought about by differences in Fe-Si and Co-Si bond lengths. As pointed out in Sec. III D, the effect of these distortions is clearly observed by means of XPD in the form of a marked reduction in photoelectron diffraction anisotropy. Thus it appears that a substantial decrease in (111)-reflection intensity may be attributed to static positional as well as chemical disorder brought about by the Fe. However, the relevant reduction in (111) reflection intensity cannot account by itself for the observed reduction. This is supported by self-consistent total-energy calculations for a ternary $Co_{1-x}Fe_xSi_2$ alloy in CaF_2 form, showing a fairly small variation of the mean Fe-Si and Co-Si distances as a function of x.[21] Moreover, XPD indicates that CaF_2-type order disappears at large Fe contents ($x \leqslant 0.75$). Hence a part of the decrease in diffraction intensity $I(x)$ must be mainly attributed to a loss of CaF_2-type order in the vacancy network, i.e., an evolution toward a defected CsCl-type structure in agreement with XPD data. An order parameter $P(x)$ can be obtained from experiment by $\sqrt{[I(x)/I_0]}$. This parameter as a function of Fe content x is displayed in Fig. 12. One can readily show that, in a model where α is the fraction of the metal atoms occupying ''wrong'' CsCl-type sites, i.e., octahedral interstitial sites in the ideal CaF_2-type structure, $P = 1 - 2\alpha$ if one neglects the contribution of disorder to the reduction of (111)-reflection intensity. Keeping in mind that the disorder contribution is actually not negligible, α is less than 10–15 % for $x \leqslant 0.50$, i.e., the CaF_2-type order is largely preserved. Hence XRD demonstrates that Co-rich films annealed at 650 °C adopt a structure close to that of CaF_2-type $CoSi_2$. Near $x = 0.85$, however, the Fe-rich layers crystallize in a CsCl-type structure with a metal atomic arrangement deviating only slightly from statistical distribution observed in low-temperature CsCl-type $FeSi_2$ ($\alpha \approx 0.50$).

Finally, note that the decrease of the order parameter P beyond $x = 0.50$ seem to be accompanied by a reduction of the (111)-interplane distance. This reduction is shown in Fig. 11 by a sizable shift of the diffraction angle $\Theta(\approx 0.13°)$ toward higher values. However, intensity of the silicide (111) reflection is too small, as compared to the substrate one, to extract an accurate angular position and (111)-interplane distance for $x \geqslant 0.50$. Actually, we cannot determine the lattice parameter or amount of strain in silicide films on the grounds of the present data, since such measurements give only information on the change of lattice constant
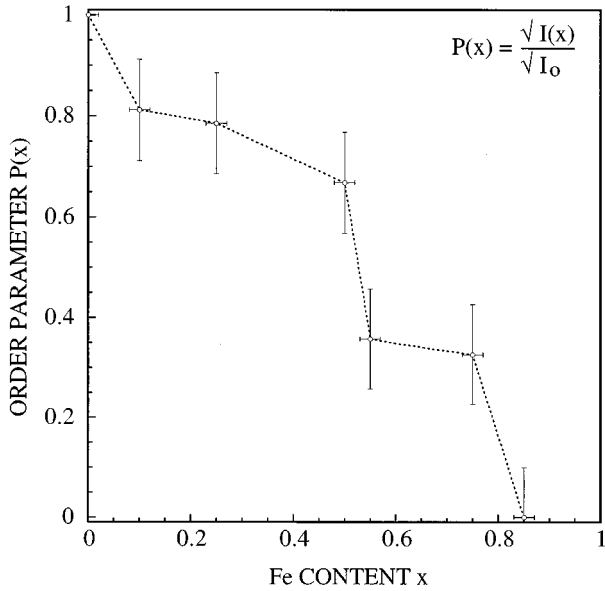
FIG. 12. Evolution of the order parameter $P(x)$ estimated by XRD (111)-reflection intensities of $Co_{1-x}Fe_xSi_2$ ($0 \leq x \leq 0.85$) annealed at 650 °C shown in Fig. 11.

perpendicular to the substrate. Note, however, that the Co-rich silicides ($x \leq 0.50$) exhibit an interplane distance d_{111} close to that of the $CoSi_2$ one. More accurate XRD measurements, including both fundamental (CsCl type) and super-structure (CaF_2 type) reflections, are underway.

F. Si 2p core-level XPS

Figure 13 displays XPS spectra of the monochromatized Al $K\alpha$-excited Si $2p$ core levels for various epitaxial $Co_{1-x}Fe_xSi_2$ silicides annealed at 400 and 650 °C. In low-temperature processed films (<400 °C), core-level binding-energy shifts do not occur as a function of the Fe-to-Co ratio. The observed binding-energy position is characteristic of Si $2p$ in binary $FeSi_{1+x}$ and $CoSi_{1+x}$ ($0 \leq x \leq 1$) films with CsCl structure.[7,33] This Si $2p$ binding energy measured on $Co_{1-x}Fe_xSi_2$ silicides of defected CsCl types means that sub-stituting Fe for Co atoms does not substantially change the Si $2p$ binding energy. Upon annealing at 650 °C, the Si $2p$ core level shifts toward lower binding energies depending on the Fe content x. In the case of $CoSi_2$ ($x=0$), the structural transition from CsCl phase to CaF_2-type phases results in a Si $2p$ core-level shift to lower binding energies of about 0.40 eV, as shown in Fig. 13, in agreement with previous work.[7] In the case of ternary films, the Si $2p$ binding energy observed in Co-rich films ($x \leq 0.50$) coincides with that in CaF_2-type $CoSi_2$. This is again consistent with the formation of a fairly well-ordered CaF_2-type phase, as revealed by XPD and XRD. In particular, in agreement with the very low deviations ($\alpha < 0.10$) from perfect CaF_2-type order ($\alpha = 0$), the electronic properties of Co-rich films are similar to those of CaF_2-type $CoSi_2$. Furthermore, it is noteworthy that the spin-orbit-split Si $2p_{1/2}$–Si $2p_{3/2}$ doublet is fairly well resolved, which definitely excludes a CsCl-CaF_2-type phase separation. The small broadening observed in the Si $2p$ dou-blet components may be attributed to the chemical and rel-evant static disorder (different Co-Si and Fe-Si bond lengths)
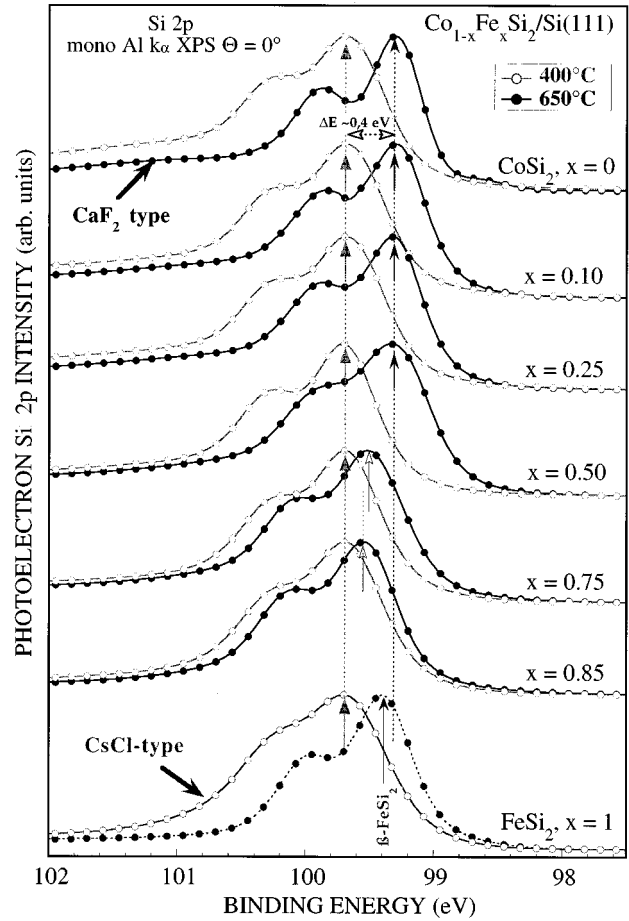

FIG. 13. Si $2p$ core levels measured from various $Co_{1-x}Fe_xSi_2/Si(111)$ annealed at 400 °C (open circles) and 650 °C (solid circles). All lines were recorded at normal emission ($\Theta = 0°$) using a monochromatized Al $k\alpha$ source (1486.6 eV). The spectra are normalized to the same maxima intensity.

in ternary $Co_{1-x}Fe_xSi_2$ silicides with respect to binary $CoSi_2$. For Fe contents $0.75 \leq x \leq 0.85$, the Si $2p$ core level adopts a binding-energy position intermediate between CsCl and CaF_2-type ones, in line with the structural evolution to-ward defected CsCl type found by XPD and XRD. However, the Si $2p$ spin-orbit-split doublet still remains fairly well resolved without substantial overall broadening, again point-ing toward single homogeneous phase formation. Actually, these Si $2p$ core-level spectra could not be reproduced by a weighted sum of Si $2p$ core lines from CsCl-type $FeSi_2$ and CaF_2-type $CoSi_2$ films.

IV. SUMMARY AND CONCLUSIONS

Using codeposition, we have shown that metastable me-tallic $Co_{1-x}Fe_xSi_2$ disilicides can be epitaxially grown on Si(111) with all compositions ranging from $FeSi_2$ to $CoSi_2$. Fe $2p_{3/2}$ and Co $2p_{3/2}$ XPD measurements clearly demonstrate that the as-codeposited disilicides adopt essen-tially the same ordered cubic structure of CsCl type with random vacancies, i.e., a structure that can be deduced from the well-known metastable defected CsCl type $FeSi_2$ by pro-gressively replacing at random Fe atoms by Co ones. This

defected CsCl-type phase is stable up to 400 °C. Upon annealing at 650 °C, 100-Å-thick films with a Co content less than 15% are invariably transformed into a semiconducting phase made of Co-doped orthorhombic β-FeSi$_2$. However, the cubic structure and metallic character are preserved as soon as the Co content exceeds about 15% ($x \leq 0.85$). Phase separation apparently does not take place. XPD measurements indicate that at least part of the Fe adopts an environment close to that in defected CsCl-type FeSi$_2$, while the local environment of Co is essentially of CaF$_2$ and defected CsCl types in Co-rich ($x \leq 0.50$) and Fe-rich films (0.50 $< x \leq 0.85$), respectively. XRD data confirm that Co$_{1-x}$Fe$_x$Si$_2$ disilicides annealed at 650 °C exhibit partial CaF$_2$ long-range order. The order parameter vanishes by x = 0.85, but increases with increasing Co content. Thus both XPD and XRD results indicate that Fe does not merely substitute for Co atoms in a perfect CaF$_2$-type CoSi$_2$ structure even in Co-rich samples. Therefore, we believe that it is not possible to stabilize a 100-Å-thick film of γ-FeSi$_2$, i.e., with a perfect CaF$_2$-type structure. Actually, in Fe-rich samples ($x > 0.50$) even the Co resides in an essentially defected

CsCl-type environment rather than CaF$_2$-type one, a result that strongly suggests that CaF$_2$-type order is not a favorable atomic arrangement in Fe-rich silicides and hence, *a fortiori*, in FeSi$_2$. Thus it is apparent that the γ-FeSi$_2$ phase may be formed only under very special circumstances such as in ultrathin films, and/or that the CaF$_2$-type order of the metal vacancies represents only a slight deviation from random (CsCl-type) distribution. Finally, it is interesting to note that, after annealing at 650 °C, the local atomic structure is definitively different for Co and Fe species, in particular in Co-rich samples. This emphasizes the role of local chemical-bonding effects, and suggests attractive nearest-neighbor interaction for Fe-Fe pairs and a repulsive one for Co-Co or Co-Fe pairs. A coupled EXAFS-XRD investigation to obtain more insight into short versus long-range order in Co$_{1-x}$Fe$_x$Si$_2$ silicides is presently underway in our laboratory.

[1] S. Muratake, M. Vatanabe, T. Suemasu, and M. Asada, Electron. Lett. **28**, 1002 (1992).

[2] T. Suemasu, M. Vatanabe, M. Asada, and N. Suzuki, Electron. Lett. **28**, 11 433 (1992).

[3] T. Suemasu, Y. Kohno, N. Suzuki, M. Vatanabe, and M. Asada, IEEE Int. Electron Devices Meeting Tech. Digest. **24**, 553 (1993).

[4] T. Suemasu, Y. Kohno, W. Saitoh, N. Suzuki, M. Vatanabe, and M. Asada, Jpn. J. Appl. Phys. **33**, L1762 (1992).

[5] R. T. Tung, J. C. Bean, J. M. Poate, and D. C. Jacobson, Appl. Phys. Lett. **40**, 684 (1982).

[6] P. Y. Dusausoy, J. Protas, R. Wadji, and B. Roques, Acta Crystallogr. B **27**, 1209 (1971).

[7] C. Pirri, S. Hong, M. H. Tuilier, P. Wetzel, G. Gewinner, and R. Cortès, Phys. Rev. B **53**, 1368 (1996).

[8] S. Hong, C. Pirri, P. Wetzel, D. Bolmont, and G. Gewinner, Appl. Surf. Sci. **90**, 66 (1995).

[9] H. von Känel, K. A. Mäder, E. Müller, N. Onda, and H. Sirringhaus, Phys. Rev. B **45**, 13 807 (1992).

[10] J. Chevrier, P. Stocker, Le Thahn Vinh, J. M. Gay, and J. Derrien, Europhys. Lett. **22**, 449 (1993).

[11] X. W. Lin, M. Behar, J. Desimoni, H. Bernas, J. Washburn, and Z. Liliental-Weber, Appl. Phys. Lett. **63**, 105 (1993).

[12] N. Jedrecy, A. Waldhauer, M. Sauvage-Simkin, R. Pinchaux, and Y. Zheng, Phys. Rev. B **49**, 4725 (1994).

[13] I. Berbezier, J. Chevrier, and J. Derrien, Surf. Sci. **315**, 27 (1994).

[14] N. Onda, J. Henz, E. Müller, K. A. Mäder, and H. von Känel, Appl. Surf. Sci. **56-58**, 421 (1992).

[15] M. C. Bost and J. E. Mahan, J. Appl. Phys. **58**, 2696 (1985).

[16] W. Z. Shen, S. C. Shen, W. G. Tang, and L. W. Wang, J. Appl. Phys. **78**, 4793 (1995).

[17] C. Giannini, S. Lagomarsino, F. Scanrinci, and P. Castrucci, Phys. Rev. B **45**, 8822 (1992).

[18] N. E. Christensen, Phys. Rev. B **42**, 7148 (1990).

[19] L. Miglio and G. Malegori, Phys. Rev. B **52**, 1448 (1995).

[20] S. Teichert, R. Kilper, T. Franke, J. Erben, P. Häussler, W. Henrion, H. Lange, and D. Panknin, Appl. Surf. Sci. **91**, 56 (1995).

[21] N. Motta and N. E. Christensen, Phys. Rev. B **43**, 4902 (1991).

[22] Z. Tan, F. Namava, S. M. Heald, and J. I. Budnick, Appl. Phys. Lett. **63**, 791 (1993).

[23] J. Tavares, H. Bender, M. F. Wu, A. Vantomme, G. Langouche, and C. Lin, Appl. Phys. Lett. **67**, 986 (1993).

[24] L. Haderbache, P. Wetzel, C. Pirri, J. C. Peruchetti, D. Bolmont, and G. Gewinner, Phys. Rev. B **39**, 1422 (1989).

[25] S. Hong, P. Wetzel, D. Bolmont, G. Gewinner, and C. Pirri, J. Appl. Phys. **78**, 5404 (1995).

[26] H. von Känel, C. Schwarz, S. Goncalves-Conto, and E. Müller, Phys. Rev. Lett. **74**, 1163 (1995).

[27] G. Gewinner, U. Kafader, P. Wetzel, and C. Pirri, J. Electron. Spectrosc. Relat. Phenom. **67**, 387 (1994), and references therein.

[28] Scott A. Chambers, Surf. Sci. Rep. **16**, 261 (1992), and references therein.

[29] U. Kafader, P. Wetzel, C. Pirri, and G. Gewinner, Appl. Surf. Sci. **70-71**, 573 (1992).

[30] N. Cherief, C. D'Anterroches, R. C. Cinti, T. A. Nguyen, and J. Derrien, Appl. Phys. Lett. **55**, 1671 (1989).

[31] C. Pirri, M. H. Tuilier, P. Wetzel, S. Hong, D. Bolmont, G. Gewinner, R. Cortès, and O. Heckmann, Phys. Rev. B **51**, 2302 (1995).

[32] Giovanna Malegori and Leo Miglio, Phys. Rev. B **48**, 9223 (1993).

[33] S. Hong, U. Kafader, P. Wetzel, G. Gewinner, and C. Pirri, Phys. Rev. B **51**, 17 667 (1995).